Journal of Biomedical Optics

SPIEDigitalLibrary.org/jbo

Multiphoton microscopy can visualize zonal damage and decreased cellular metabolic activity in hepatic ischemia-reperfusion injury in rats

Camilla A. Thorling
Xin Liu
Frank J. Burczynski
Linda M. Fletcher
Glenda C. Gobe
Michael S. Roberts

SPIE

Multiphoton microscopy can visualize zonal damage and decreased cellular metabolic activity in hepatic ischemia-reperfusion injury in rats

Camilla A. Thorling,[a,b] Xin Liu,[a] Frank J. Burczynski,[c] Linda M. Fletcher,[a,d] Glenda C. Gobe,[a] and Michael S. Roberts[a,b]
[a]The University of Queensland, School of Medicine, Woolloongabba, Queensland, 4102, Australia
[b]University of South Australia, School of Pharmacy and Biomedical Sciences, Adelaide, Australia
[c]University of Manitoba, Faculty of Pharmacy, Canada
[d]Princess Alexandra Hospital, Department of Gastroenterology and Hepatology, Brisbane, Australia

Abstract. Ischemia-reperfusion (I/R) injury is a common occurrence in liver surgery. In orthotopic transplantation, the donor liver is exposed to periods of ischemia and when oxygenated blood is reintroduced to the liver, oxidative stress may develop and lead to graft failure. The aim of this project was to investigate whether noninvasive multiphoton and fluorescence lifetime imaging microscopy, without external markers, were useful in detecting early liver damage caused by I/R injury. Localized hepatic ischemia was induced in rats for 1 h followed by 4 h reperfusion. Multiphoton and fluorescence lifetime imaging microscopy was conducted prior to ischemia and up to 4 h of reperfusion and compared to morphological and biochemical assessment of liver damage. Liver function was significantly impaired at 2 and 4 h of reperfusion. Multiphoton microscopy detected liver damage at 1 h of reperfusion, manifested by vacuolated cells and heterogeneous spread of damage over the liver. The damage was mainly localized in the midzonal region of the liver acinus. In addition, fluorescence lifetime imaging showed a decrease in cellular metabolic activity. Multiphoton and fluorescence lifetime imaging microscopy detected evidence of early I/R injury both structurally and functionally. This provides a simple noninvasive technique useful for following progressive liver injury without external markers.
[DOI: 10.1117/1.3647597]

Keywords: liver function; multiphoton microscopy; fluorescence lifetime imaging microscopy; histology; nicotinamide adenine dinucleotide; zonation.

Paper 11298R received Jun. 13, 2011; revised manuscript received Sep. 1, 2011; accepted for publication Sep. 19, 2011; published online Oct. 27, 2011.

1 Introduction

Ischemia-reperfusion (I/R) injury of the liver is a common phenomenon and a major cause of morbidity and mortality in many clinical situations, including hepatic resection and liver transplantation.[1,2] Cellular damage in I/R injury is intensified when the transplanted liver is reperfused with blood after prolonged period(s) of ischemia in the donated liver.[3] During orthotopic liver transplantation, oxygenated blood is reintroduced to the liver resulting in oxidative stress through free radical production.[4] Hepatic injury in the transplanted liver results in intracellular adenosine triphosphate (ATP) loss, increased microvascular permeability, inflammatory cell infiltration, and potentially, cell death in the forms of apoptosis and necrosis.[5,6] As a consequence, oxidative stress may lead to graft failure and rejection of the transplanted liver.[6]

The reduced form of nicotinamide adenine dinucleotide (NADH) is essential in the production of ATP as an electron donor and a coenzyme.[7–9] ATP can be produced in two ways: 1. through glycolysis, an anaerobic process occurring in the cytoplasm; or 2. through oxidative phosphorylation, an aerobic process occurring in the mitochondria.[8] NADH can be free or protein-bound where binding occurs to a mitochondrial membrane protein, which mediates electron transfer from NADH to oxygen and results in H^+ being transported to the cytoplasm. This yields a gradient that is necessary for ATP synthesis and occurs only in the presence of oxygen.[9] Thus, bound NADH is involved in ATP synthesis in aerobic conditions.[9] The free form of NADH is mainly located in the cytoplasm, where glycolysis occurs, producing ATP without oxygen.[10] Accordingly, free and protein-bound NADH are involved in the production of ATP and changes in the ratio between the two forms gives insight into the metabolic state of a cell.[9] The metabolic state can be determined *in vivo* through the recent advances in microscopy and the inherent fluorescent properties of NADH, as has been shown in assessing the viability of excised human skin stored under various conditions.[11,12]

Multiphoton microscopy (MPM) has been utilized for the visualization of fluorescent molecules within the cell,[13] including measuring the absorption of nanoparticles into human skin.[14] MPM enables high-resolution imaging of physiology, morphology, and cell-cell interactions in live animals or intact tissue.[15] The effective resolution in MPM is far superior to confocal microscopy because fluorescence only arises from the focus.[15] Photodamage in MPM is therefore limited to the focal plane, however, the possibility of damage in this region still remains.[15] Confocal microscopy, however, uses single photon excitation resulting in broad exposure to high-energy UV and visible

Address all correspondence to: Michael S. Roberts, University of Queensland, Therapeutics Research Centre, School of Medicine, Princess Alexandra Hospital, Boulevard 35 Lv1, Ipswich Road, Woolloongabba, Queensland, 4102, Australia; Tel: +61 7 3176 5803; Fax: +61 3176 5806; E-mail: m.roberts@uq.edu.au.

1083-3668/2011/16(11)/116011/8/$25.00 © 2011 SPIE

excitation sources in the specimen above the focus plane, which could damage photosensitive samples.[16] MPM is also better suited for deep-tissue imaging compared to confocal, because the infrared light used to generate multiphoton excitation is less scattered in biological samples.[16] This results in a tightly focused beam with high-photon flux enabling deeper imaging into thick tissue while restricting photobleaching and phototoxicity.[17,18] The two or more low energy photons in MPM are simultaneously absorbed in order to excite an electron from a fluorescent molecule.[19,20] The photons have similar energies and produce an excitation equivalent to single-photon absorption possessing twice the energy.[15] The images originate at the beam focus with no out of focus background present.[17]

Fluorescence lifetime imaging microscopy (FLIM) is based on the average time it takes for an electron to return from the excited state to the ground state. It adds to the information from MPM by making it possible to resolve multiple lifetimes from decay data.[21] The advantage of FLIM is that it is dependent on excited state reactions, but independent of the concentration of the fluorescent molecule.[22] The concept of FLIM has been simply explained by Lakowicz et al. Briefly, the fluorescence intensity cannot reveal any environmental changes, such as protein binding or pH, but FLIM can.[23] Therefore, FLIM provides details about the structure and dynamics of fluorescent molecules[12] and is sensitive to changes in conformation, molecular interactions, ion concentrations, pH[9] and oxygen concentrations.[24] Our previous results using MPM-FLIM focused on nanoparticle and solvent uptake in both excised[14,25–27] and *in vivo*[28,29] skin. In addition, this method has been used to study fluorescein distribution and metabolism in the liver *in vivo* in rats.[14,30] In the present study, we utilized the autofluorescent properties of the liver cells to investigate cellular damage progression in I/R injury.

NADH has fluorescent properties with peak absorption at 350 nm and peak emission of approximately 450 nm.[10] The free and protein-bound forms of NADH have similar excitation and emission wavelengths, but can be separated using their distinct fluorescence lifetimes of 0.4 to 0.5 and 2.0 to 2.5 ns, respectively.[10] Nicotinamide adenine dinucleotide phosphate (NADPH) is another reducing agent used in biosynthesis of fatty acids and steroids. NADH and NADPH have the same excitation and emission wavelengths and fluorescence lifetimes, and cannot be spectrally resolved.[31] Hence, NADH and NADPH are referred to as NAD(P)H in this paper. However, NADPH has lower fluorescence intensity, lower concentration, and is roughly constant with respect to metabolic perturbations compared to NADH.[32] The influence of NADPH is therefore considered very low, although not insignificant. We have previously studied NAD(P)H in ischemic necrosis of the skin and showed that MPM-FLIM was useful for noninvasive imaging and to monitor the metabolic state of the skin.[11]

Thus, the aim of this study was to investigate whether MPM and FLIM are useful tools in detecting disease progression in I/R injury, without the need for external markers.

2 Materials and Methods

2.1 *Animals*

Male Wistar rats, purchased from the Animal Resource Centre (Perth, Western Australia), weighing approximately 300 g were used in all experiments. Studies were approved by the Animal Ethics Committee of the University of Queensland and were carried out in accordance with the legislation of Australian authorities for the care and use of experimental animals. Animals were housed in the Biological Resource Facility at the Princess Alexandra Hospital, where the temperature is maintained at 20 $\pm$ 1°C and humidity at 60 to 75%, with artificial light for 12 h (7 am to 7 pm) daily. All animals had unlimited access to food and water.

2.2 *Surgical Procedures*

Rats were anaesthetized by an initial intraperitoneal injection of xylazine 10 mg/kg and ketamine hydrochloride 80 mg/kg. Anaesthesia was maintained throughout the experiment by intraperitoneally administering ketamine (2.2 mg/100 g) and xylazine (0.25 mg/100 g). Body temperature was controlled by placing them on a heated pad set to 37°C. A midline laparotomy was performed with the left lobe of the liver exposed for imaging.

2.3 *I/R Model*

70% ischemia was induced by clamping the portal vein, hepatic artery, and bile duct supplying the median and left lobes of the liver using a microvascular clamp. After 60 min of partial ischemia, the clamp was removed to allow reperfusion in the liver. Sham rats (controls) underwent the same procedures without clamping the vessels.

2.4 *Tissue Collection*

Blood (0.2 ml) was collected from the inferior vena cava using a 30-gauge needle before ischemia induction and at 2 and 4 h of reperfusion. After the animal was euthanized at the end of 4 h reperfusion, the left and median lobes were excised, portions were either snap frozen in liquid nitrogen and stored at -70°C for later analysis of glutathione (GSH), or immersed into 10% buffered formalin for histological assessment.

2.5 *MPM-FLIM*

MPM was performed using a DermaInspect system (JenLab GmbH, Jena, Germany) equipped with an ultrashort (85 femtosecond pulse width) pulsed mode-locked 80-MHz Titanium:Sapphire MaiTai laser (Spectra Physics, Mountain View, California). For FLIM, a time correlated single photon counting 830 detector (Becker & Hickl, Berlin, Germany) was incorporated into the MPM system. The excitation wavelength was set to 740 nm for FLIM (emission range 350 to 450 nm) and 780 nm for imaging of autofluorescence. For imaging of the liver, the left lobe was placed on a small metal plate, attached to an adjustable stand that could be elevated or lowered as required. The plate was slightly raised above the intraperitoneal cavity to minimize pressure on the organs underneath. The laser power was 15 mW and a BG39 (350 to 650 nm) emission filter was used. The acquisition time for obtaining the images was 13.4 s per frame. Images were taken pre-ischemia induction, during ischemia, and at 0, 1, 2, and 4 h of reperfusion.

2.5.1 *Data analysis*

FLIM images were analyzed using SPCImage (Becker & Hickl, Berlin, Germany). Lifetime distributions for NAD(P)H were obtained by fitting photon count $F(t)$ profiles from each image to a bi-exponential decay function ($F(t) = \alpha_1 e^{-t/\tau_1} + \alpha_2 e^{-t/\tau_2}$). The reduced chi-square coefficient was used to indicate goodness-of-fit. Two lifetimes, τ_1 and τ_2 represent the "fast" and "slow" lifetimes of free and protein-bound NAD(P)H, respectively. The amplitudes α_1 and α_2 represent the relative concentration fraction of NAD(P)H, where $\alpha_1 + \alpha_2 = 100$.[12] The ratio of a_1 and a_2 is the best way to determine the free and protein-bound state of NAD(P)H, therefore showing the metabolic changes of the cell. In this study the actual ratio of α_1 and α_2 is shown. In addition, the ratio of α_1 and α_2 is also presented as pseudo color images exported from the analyzing software, where a change in color indicates a change in ratio. Actual changes in lifetimes, τ_1 and τ_2, are not shown in this study. For statistical analysis, student t-test for paired samples and one-way ANOVA with Tukey's adjustment for multiple comparisons were used. Results were considered statistically significant with a p-value ≤ 0.05.

2.6 *Histopathological Analyses*

Staining of haematoxylin and eosin (H&E), ApopTag (for apoptosis) and immunohistochemistry for ED1 (for macrophages) was performed according to standard procedure. Visualization of ApopTag and ED1 localization was facilitated with diaminobenzidine hydrochloride, which stained brown in positively-labeled cells. Fixed liver was sub-sectioned onto each slide (two to three sections at 5 μm from different slices of each liver), stained, and then scanned using an Aperio ScanScope XT slide scanning system (Aperio Technologies Inc., Vista, California) at 20× magnification. The Aperio ImageScope V10.2. software was used to visualize and score the slides. Severity of tissue damage was quantified in five areas per slide by two independent personnel using a previously described method.[33] Three sets of parameters were studied: a. cellular degeneration defined as cellular swelling and vacuolation, and reversible changes in nuclear density; b. infiltration of neutrophils, monocytes, and macrophages; and c. necrosis defined by cells showing pyknosis, karyorrhexis, karyolysis, and cytolysis. These parameters were graded as follows. Grade 1: no change from normal; Grade 2: a limited number of isolated cells (up to 5% of cells); Grade 3: groups of cells (5 to 30% of the total cell number); and Grade 4: diffuse cell damage (higher than 30% of the total cell number). In addition, zonal localization of tissue damage was recorded.

Using immunohistochemistry for ED1, the number of monocytes and macrophages were identified by counting ED1-positive cells in the sinusoids in 10 random fields per slide. Apoptotic cells were identified enzymatically using ApopTag labeling, and positive nuclei were counted in 10 random fields per region per liver slide. The three different regions were 1. periportal (cells surrounding the portal tract), 2. centrilobular (cells surrounding the central vein), and 3. midzonal (cells between the periportal and centrilobular zones).

Table 1 Alanine aminotransferase before (pre) and after ischemia induction at 2 and 4 h of reperfusion. [$^*p < 0.05$ versrus sham, $^\#p < 0.05$ versus pre. Mean (±SEM).]

	ALT (U/L) Pre	ALT (U/L) 2 h	ALT (U/L) 4 h
I/R injury ($n = 6$)	50 (±5)	1120 (±308)$^{*\#}$	1820 (±600)$^{*\#}$
Sham ($n = 4$)	40 (±7)	40 (±17)	60 (±20)

2.7 *Serum Biochemical Measurements*

Plasma concentration of alanine aminotransferase (ALT) was measured using a Hitachi 747 analyzer (Hitachi Ltd., Tokyo, Japan) in the Pathology Department at Princess Alexandra Hospital, Brisbane.

2.8 *Determination of Total Glutathione (GSH)*

GSH was determined using the Glutathione assay kit (Cayman Chemical Company). The kit is based on the reaction between GSH and DTNB [5,5′-dinitro-bis-2-(nitrobenzoic acid)], which produces a yellow colored TNB (5-thio-2-nitrobenzoic acid). The production of TNB is directly proportional to the concentration of GSH.

3 Results

3.1 *Alanine Transaminase (ALT)*

The model of ischemia used resulted in extensive liver damage as measured by increased liver ALT. ALT was significantly ($p < 0.05$) increased at 2 (1120 ± 308 U/L) and 4 h (1820 ± 600 U/L) of reperfusion compared to sham (Table 1).

3.2 *Oxidative Stress*

As a measure of oxidative stress, GSH concentration at 4 h I/R was determined in excised livers. GSH concentration was significantly ($p < 0.05$) reduced in the I/R group compared to sham (Table 2).

3.3 *Histopathological Findings*

Mild to moderate structural alterations in the liver were found in the I/R injury group [Fig. 1(a)]. Cellular vacuolation was present in all sections from the I/R injury group, with scores from 2 to 4 for cell degeneration. Some inflammatory cell infiltration was

Table 2 Levels of oxidative stress were measured by glutathione concentration in the liver at 4 h of reperfusion in I/R injury and compared to sham rats (±SEM). ($^*p < 0.05$ versus sham.)

	Glutathione concentration (μmoles/g liver)
I/R injury ($n = 6$)	1460 (±100)
Sham ($n = 5$)	550 (±130)*

Table 3 Semi-quantitative categorization of the morphological injury parameters in liver tissue after I/R injury. Scoring from 1 to 4, where 1 is no and 4 is a major change (±SEM). ($^{*}p < 0.05$ versus sham.)

	Sham ($n = 5$)	I/R injury ($n = 6$)
Cell degeneration	1.1 (±0.08)	2.0 (±0.3)*
Inflammatory cell infiltration		
–Neutrophils	1.0 (±0)	1.3 (±0.1) *
–Monocytes/macrophages	1.0 (±0)	1.4 (±0.1)*
Necrosis	1.0 (±0)	1.3 (±0.2)

present in sham and I/R rats at 4 h of reperfusion (Table 3). There was no statistical difference in the number of monocytes and macrophages, stained with ED1, as seen in Fig. 1(b). The number of monocytes and macrophages tended to be slightly decreased in I/R injury (240 ± 50) compared to the sham group (310 ± 70), however this was not significantly different.

The number of apoptotic cells was statistically increased in the centrilobular and midzonal regions compared to the same regions in the sham group [Fig. 1(c), Table 4] ($p < 0.05$). There was a slight increase in the number of apoptotic cells in the periportal region, however, not statistically significant (Table 4).

3.4 *MPM-FLIM*

The autofluorescence of the liver *in vivo* was imaged with high resolution at 0, 1, 2, and 4 h of reperfusion. Figure 2 shows representative images from one rat in the I/R injury group and one in the sham group. A large dark area is seen at 4 h of reperfusion in the I/R group, which cannot be seen to the same extent in sham rats (Fig. 2). In addition, vacuoles were formed within the cells in some of the images taken after ischemia, and this was not seen in sham rats. Figure 3(a) shows an example of such a phenomenon at 1 h of reperfusion. The same experiment was done using a lower magnification objective to visualize the entire liver acinus. Figure 3(b) shows sample images from one rat before the start of ischemia (control) and at 4 h of reperfusion. Dark patches are evident in different areas around the acinus at 4 h of reperfusion that was not seen in the sham group.

FLIM measures the relative contribution of free/bound NAD(P)H in the liver *in vivo* in I/R injury. The relative concentrations of free ($\alpha 1$) and bound ($\alpha 2$) NAD(P)H were calculated and plotted against time (Fig. 4). The ratio of free/bound

Table 4 Number of apoptotic cells in the three regions of the liver lobule. ApopTag-labeled nuclei were counted in 10 different fields per zone of the liver acinus (mean ± SEM). ($^{*}p < 0.05$ versus I/R injury, $^{\#}p < 0.05$ versus periportal and centrilobular.)

	Periportal	Midzonal	Centrilobular
I/R injury ($n = 6$)	17.8 ± 4.9	89.5 ± 19.5$^{\#}$	43.2 ± 12.8
Sham ($n = 5$)	7.4 ± 2.5	5.2 ± 1.7*	2.0 ± 0.6*

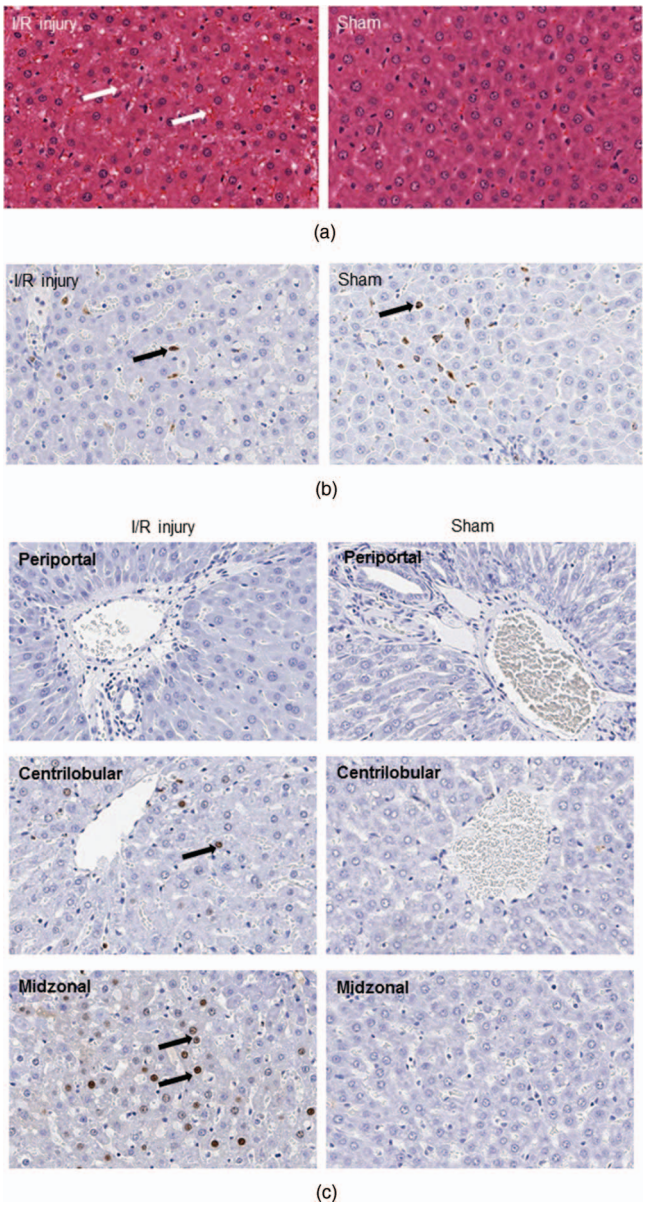

Fig. 1 Histology of liver tissue after I/R injury. (a) H&E stained liver tissue shows increased vacuolation in the I/R group. White arrow indicates vacuoles. (b) ED1 stained liver showing monocytes and macrophages stained in brown. Black arrows show inflammatory cells. (c) ApopTag stained liver showing apoptotic cells in the three different regions in the liver lobule, periportal, centrilobular, and midzonal. Black arrows indicate apoptotic cells. Magnification 20×, sham $n = 5$, I/R $n = 6$.

NAD(P)H was significantly increased after 2 and 4 h of reperfusion [$p < 0.05$; Fig. 4(a)]. This increase was due to a statistical increase and decrease in the relative concentration of free [Fig. 4(b)] and bound [Fig. 4(c)] NAD(P)H, respectively.

Another way of showing the relative concentration of free/bound NAD(P)H is to false color the images obtained from the FLIM analysis. Figure 4(d) shows sample images from one rat in the I/R injury group and another from the sham group. The color of the images (from blue to red) indicates the ratio of free/bound NAD(P)H. At 1, 2, and 4 h of reperfusion there is a shift in the color to yellow, indicating an increase in the ratio as seen in the color bar.

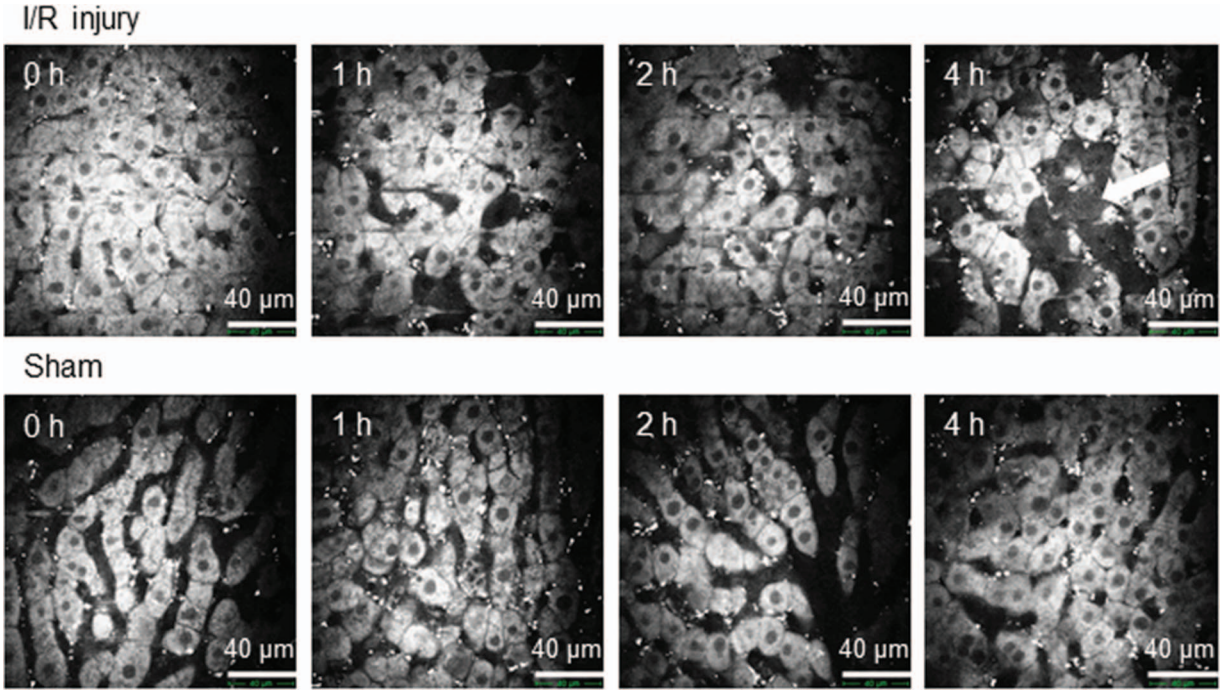

Fig. 2 Multiphoton microscopy images of liver *in vivo* in I/R injury at various reperfusion time points compared to sham rats. The white arrow indicates a large dark area not seen in the sham group.

4 Discussion

Fluorescence microscopy can provide valuable information on tissue morphology without the need for histological assessment.[34] The technique utilizes the autofluorescence of tissue components such as NADH,[34] flavine adenine dinucleotide,[35] and other flavoproteins.[36] However, most previous studies have been conducted *in vitro* with only a few studies performed on live animals.[34] External markers for liver damage such as rhodamine 123 and propidium iodide have previously been used to study mitochondrial permeability transition and necrosis, respectively.[37,38] However, the aims of this study were to investigate whether we could use the autofluorescent properties of the tissue to detect cell damage using MPM in combination with FLIM. MPM uses a high-pulsed laser, which provides low average energy received by the sample imaged.[39] In addition, MPM restricts excitation of a fluorescent molecule to the focal plane of the microscope.[39] Consequently, MPM significantly improves the quality of images acquired from biological tissue, by reducing photodamage and photobleaching of tissue compared to conventional fluorescence microscopy.[17,19,20]

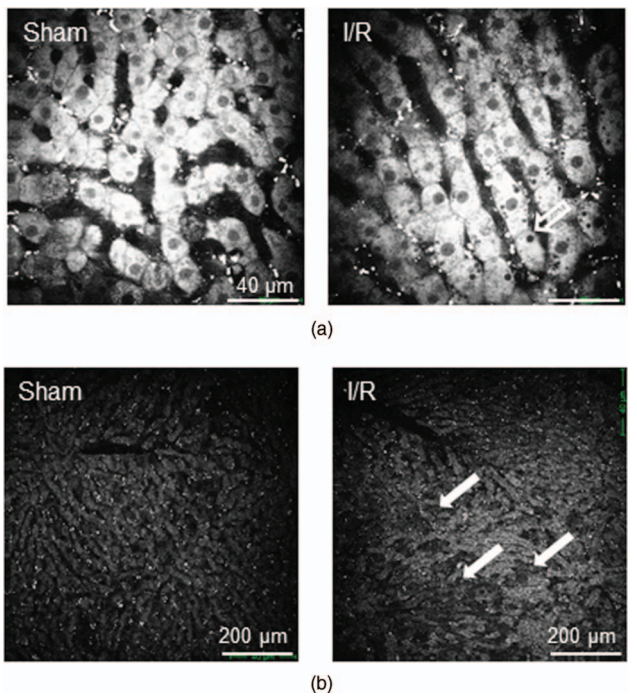

Fig. 3 Multiphoton microscopy images of liver tissue on cellular and acinus levels. (a) Images recorded at 1 h of reperfusion in the I/R group using high and (b) at 4 h using low magnifications (40× and 10×, respectively). White opened arrow indicates vacuolation and solid arrows indicate increased dark areas.

The model of ischemia used resulted in extensive liver damage, as measured by increased liver ALT (Table 1) and depletion of one of the cellular defence mechanisms against free radicals (GSH) (Table 2). Early ischemia reperfusion injury has in previous studies resulted in similar increases of ALT and GSH levels.[40,41] It has been shown that this injury is mediated through a release in free radicals both within the cell and outside through Kupffer cell activation.[42]

It was evident that hepatocytes became vacuolated after 1 h of reperfusion, indicating cellular stress[43] that was not evident in sham rats [Fig. 3(a)]. In addition to the fluorescence intensity images, traditional H&E staining of the liver also showed vacuolation in the hepatocytes [Fig. 1(a)], which confirms the findings of Sireli et al., who reported swollen hepatocytes with vacuolated cytoplasm during I/R injury.[44] Additional immunohistological staining for monocytes and macrophages showed no increase in the number of these inflammatory cells in the I/R

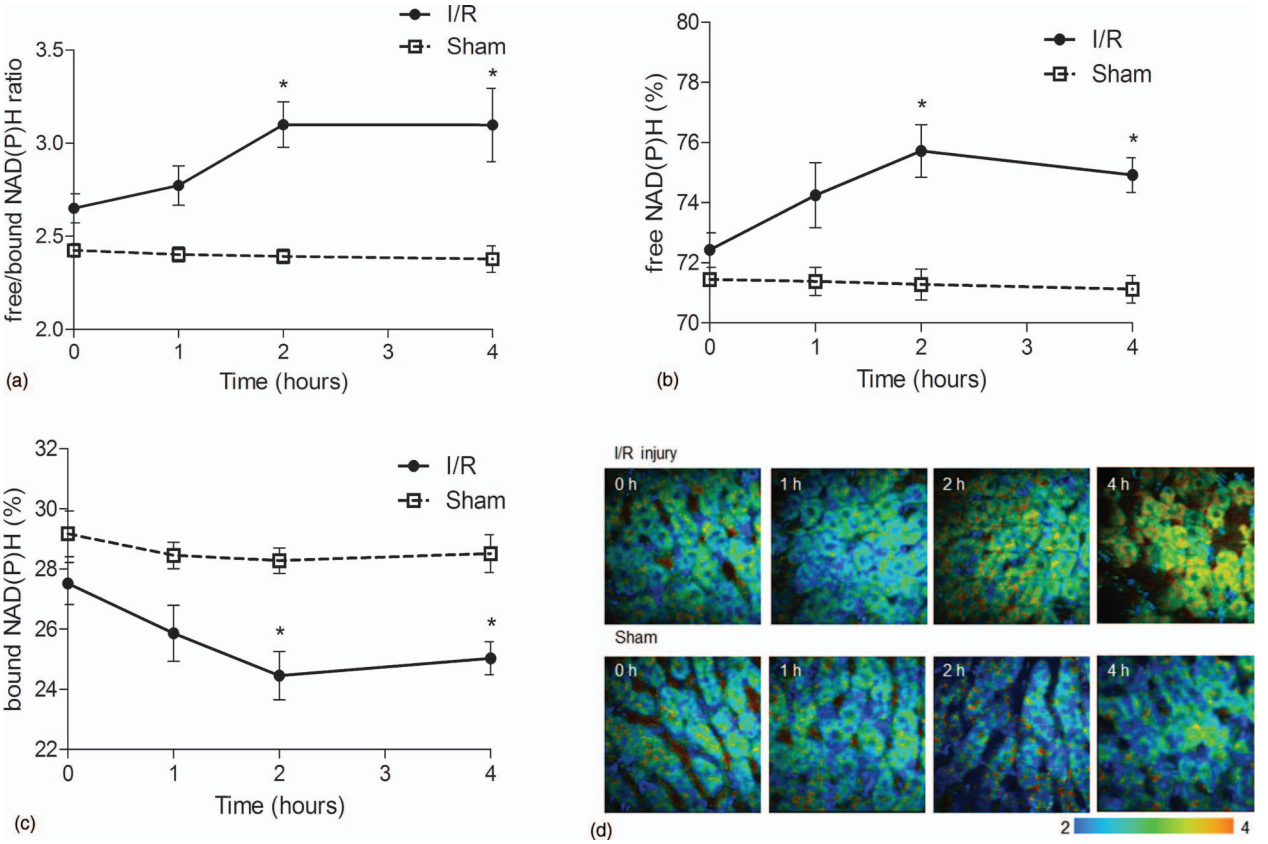

Fig. 4 Changes in free and bound levels of NAD(P)H recorded by fluorescence lifetime imaging microscopy. (a) Ratio of free/bound NAD(P)H was significantly increased at 2 and 4 h of reperfusion in the I/R group compared to sham. This increase was shown to be due to an increase in (b) free NAD(P)H and a decrease in (c) bound NAD(P)H, respectively. (d) Relative concentration of free/bound NAD(P)H is expressed in pseudo color images. The color of the cells in I/R injury shifts toward yellow over time indicating an increase in the ratio of free/bound NAD(P)H. This increase was not seen in sham rats. *$p < 0.05$ versus sham ($n = 4$).

injury group. Since the liver has its own macrophages, called Kupffer cells, that line the sinusoids, it is probable that ED1 would stain those as well.[45] The number of Kupffer cells should stay constant in the liver, which would explain why the number of stained monocytes and macrophages are similar in both groups.[45]

In the images recorded by MPM, large dark areas were noticed at 4 h of reperfusion in the I/R injury group that could not be seen in any of the sham rats. A decrease in fluorescence is most likely due to a decrease in NAD(P)H fluorescence, which occurs in cell death.[46] Using high magnification, this dark area was seen in three out of four I/R animals. We, therefore, suspected a zonal spread in the liver damage and investigated this at lower magnification. While the results showed variation in intensity of light and dark, the dark areas of the liver were localized away from the periportal region. To confirm the heterogenic spread in the damage the harvested livers were histopathologically analyzed. ApopTag stained cells, staining DNA damaged nuclei,[47] were significantly increased in the centrilobular and midzonal regions, but not in the periportal region. Early ischemia reperfusion injury induces a burst of free radicals,[42] which in turn cause DNA strand breaks in the nuclei of the cells. Although the strand breaks may predetermine progress to apoptosis, they may also be repairable and so the injury is reversible. ApopTag enzymatic labeling, by its very nature,[48] will label both repairable and apoptosis-inducing DNA strand breaks. The nuclei that stained positive with the ApopTag as shown in Fig. 1(c), but had apparently normal structure after the (4 h) reperfusion, may ultimately take either pathway. Our group is now focusing on the long term damage of hepatic I/R injury. A review of the literature suggests that there is an altered distribution of zonal damage associated with different liver diseases. For example, hypoxia and free radical production have been reported to affect cells around the central vein in alcohol induced liver injury,[49] whereas midzonal parenchymal cells were more susceptible to oxidative stress in cancer and cirrhosis.[50] Furthermore, liver damage was more pronounced in centrilobular and midzonal regions after acetaminophen administration.[51]

The brighter parts of the images are likely explained by an increase in NAD(P)H concentration during I/R injury. Barbiro et al. showed a significant increase in NADH levels in hepatic I/R injury,[52] and similar results have been reported in hypoxic hepatocytes *in vitro*.[53] NADH loses fluorescence during oxidation to NAD(P)+, thus NAD(P)H fluorescence can be used to monitor metabolism.[54] However, measuring total concentration of NAD(P)H can be misleading because it is not possible to know whether the fluorescence is derived from free or protein-bound NAD(P)H.[32] FLIM is, therefore, a better probe for studying changes in NAD(P)H because the lifetime of the molecule is significantly enhanced with binding.[32] The amplitude (α) can be related to the concentration of NAD(P)H[9,54,55] and the ratio of free/bound ($\alpha 1/\ \alpha 2$) NAD(P)H was calculated at different

reperfusion time points. A significant increase was seen at 2 and 4 h of reperfusion [Figs. 4(a) and 4(d)]. This was attributed to an increase in free and a decrease in bound NAD(P)H [Figs. 4(b) and 4(c)]. It is possible that the increase in free/bound NAD(P)H seen in this study is attributable to the Pasteur effect, where cellular respiration is shifted to glycolysis, producing ATP in anaerobic conditions.[56,57] An increase in glycolysis leads to an increase in lactic acid production,[35] which was previously reported in pig liver during warm ischemia.[58] In addition, increased levels of lactic acid were seen in patients undergoing hepatectomy, which further coincides with the theory of shift to glycolysis in I/R injury of the liver.[59] Our group has previously shown an increase in free NAD(P)H in skin after zinc oxide application *in vivo*.[28]

In conclusion, liver damage associated with I/R injury, with up to 4 h of reperfusion, was structurally characterized by a zonal distribution of vacuolated and degenerating hepatocytes, increased apoptosis, and mild necrosis. The damage was mainly localized in the midzonal region. MPM was able to detect both cellular degeneration and the zonal spread of damage, by showing irregular fluorescence intensity of the hepatocytes. FLIM added to these results by detecting changes in cellular respiration, which was attributed by an increase in free NAD(P)H and a decrease in bound NAD(P)H in I/R injury. This is an important and novel finding in that it allows us to follow disease development without the administration of an external marker *in vivo*.

Acknowledgments

National Health and Medical Research Council (NHMRC #569710) is acknowledged for funding this project. Clay Winterford and colleagues at Queensland Institute of Medical Research (QIMR) prepared the histology and immunohistochemistry. Goce Dimeski and colleagues at Queensland Pathology Services, Princess Alexandra Hospital, conducted ALT measurements. Professor Yan Yang, Department of Pharmacology, Anhui Medical University, Hefei, China, is thanked for helping to set up the animal model and for professional advice.

References

1. Y. Takamatsu, K. Shimada, K. Yamaguchi, S. Kuroki, K. Chijiiwa, and M. Tanaka, "Inhibition of inducible nitric oxide synthase prevents hepatic, but not pulmonary, injury following ischemia-reperfusion of rat liver," *Dig. Dis. Sci.* **51**(3), 571–579 (2006).
2. J. Baumann, S. Ghosh, T. Szakmany, G. Jancso, A. Ferencz, E. Roth, and L. Bogar, "Short-term effects of N-acetylcysteine and ischemic preconditioning in a canine model of hepatic ischemia-reperfusion injury," *Eur. Surg. Res.* **41**(2), 226–230 (2008).
3. M. L. Hart, C. Much, D. Kohler, J. Schittenhelm, I. C. Gorzolla, G. L. Stahl, and H. K. Eltzschig, "Use of a hanging-weight system for liver ischemic preconditioning in mice," *Am. J. Physiol. Gastrointest. Liver Physiol.* **294**(6), G1431–G1440 (2008).
4. R. Chavez-Cartaya, N. V. Jamieson, P. Ramirez, J. Marin, and G. Pino-Chavez, "Free radical scavengers to prevent reperfusion injury following experimental warm liver ischaemia. Is there a real physiological benefit?," *Transpl. Int.* **12**(3), 213–221 (1999).
5. G. Sener, O. Tosun, A. O. Sehirli, A. Kacmaz, S. Arbak, Y. Ersoy, and G. Ayanoglu-Dulger, "Melatonin and N-acetylcysteine have beneficial effects during hepatic ischemia and reperfusion," *Life Sci.* **72**(24), 2707–2718 (2003).
6. D. Crenesse, J. Gugenheim, J. Hornoy, K. Tornieri, M. Laurens, B. Cambien, G. Lenegrate, R. Cursio, G. De Souza, P. Auberger, C. Heurteaux, B. Rossi, and A. Schmid-Alliana, "Protein kinase activation by warm and cold hypoxia-reoxygenation in primary-cultured rat hepatocytes-JNK(1)/SAPK(1) involvement in apoptosis," *Hepatology* **32**(5), 1029–1036 (2000).
7. T. Nishikawa, D. Edelstein, X. L. Du, S. Yamagishi, T. Matsumura, Y. Kaneda, M. A. Yorek, D. Beebe, P. J. Oates, H. P. Hammes, I. Giardino, and M. Brownlee, "Normalizing mitochondrial superoxide production blocks three pathways of hyperglycaemic damage," *Nature* **404**(6779), 787–790 (2000).
8. M. Erecinska and D. F. Wilson, "Regulation of cellular energy metabolism," *J. Membr. Biol.* **70**(1), 1–14 (1982).
9. V. V. Ghukasyan and F.-J. Kao, "Monitoring cellular metabolism with fluorescence lifetime of reduced nicotinamide adenine dinucleotide," *J. Phys. Chem. C* **113**, 11532–11540 (2009).
10. D. K. Bird, L. Yan, K. M. Vrotsos, K. W. Eliceiri, E. M. Vaughan, P. J. Keely, J. G. White, and N. Ramanujam, "Metabolic mapping of MCF10A human breast cells via multiphoton fluorescence lifetime imaging of the coenzyme NADH," *Cancer Res.* **65**(19), 8766–8773 (2005).
11. W. Y. Sanchez, T. W. Prow, W. H. Sanchez, J. E. Grice, and M. S. Roberts, "Analysis of the metabolic deterioration of *ex vivo* skin from ischemic necrosis through the imaging of intracellular NAD(P)H by multiphoton tomography and fluorescence lifetime imaging microscopy," *J. Biomed. Opt.* **15**(4), 046008 (2010).
12. M. S. Roberts, Y. Dancik, T. W. Prow, C. A. Thorling, L. L. Lin, J. E. Grice, T. A. Robertson, K. Konig, and W. Becker, "Non-invasive imaging of skin physiology and percutaneous penetration using fluorescence spectral and lifetime imaging with multiphoton and confocal microscopy," *Eur. J. Pharm. Biopharm.* **77**(3), 469–488 (2011).
13. Y. Liu, H. C. Chen, S. M. Yang, T. L. Sun, W. Lo, L. L. Chiou, G. T. Huang, C. Y. Dong, and H. S. Lee, "Visualization of hepatobiliary excretory function by intravital multiphoton microscopy," *J. Biomed. Opt.* **12**(1), 014014 (2007).
14. M. S. Roberts, M. J. Roberts, T. A. Robertson, W. Sanchez, C. Thorling, Y. Zou, X. Zhao, W. Becker, and A. V. Zvyagin, "*In vitro* and *in vivo* imaging of xenobiotic transport in human skin and in the rat liver," *J. Biophotonics* **1**(6), 478–493 (2008).
15. W. R. Zipfel, R. M. Williams, and W. W. Webb, "Nonlinear magic: multiphoton microscopy in the biosciences," *Nature Biotechnol.* **21**(11), 1368–1376 (2003).
16. M. T. Butko, M. Drobizhev, N. S. Makarov, A. Rebane, B. C. Brinkman, and J. G. Gleeson, "Simultaneous multiple-excitation multiphoton microscopy yields increased imaging sensitivity and specificity," *Bmc Biotechnol.* **11**(20), (2011).
17. R. M. Williams, W. R. Zipfel, and W. W. Webb, "Multiphoton microscopy in biological research," *Curr. Opin. Chem. Biol.* **5**(5), 603–608 (2001).
18. K. Konig, "Multiphoton microscopy in life sciences," *J. Microsc.* **200**, 83–104 (2000).
19. K. W. Dunn and P. A. Young, "Principles of multiphoton microscopy," *Nephron. Exp. Nephrol.* **103**(2), e33–e40 (2006).
20. H. S. Lee, Y. Liu, H. C. Chen, L. L. Chiou, G. T. Huang, W. Lo, and C. Y. Dong, "Optical biopsy of liver fibrosis by use of multiphoton microscopy," *Opt. Lett.* **29**(22), 2614–2616 (2004).
21. N. D. Evans, L. Gnudi, O. J. Rolinski, D. J. Birch, and J. C. Pickup, "Glucose-dependent changes in NAD(P)H-related fluorescence lifetime of adipocytes and fibroblasts *in vitro*: potential for non-invasive glucose sensing in diabetes mellitus," *J. Photochem. Photobiol., B* **80**(2), 122–129 (2005).
22. P. I. H. Bastiaens and A. Squire, "Fluorescence lifetime imaging microscopy: spatial resolution of biochemical processes in the cell," *Trends Cell Biol.* **9**(2), 48–52 (1999).
23. J. R. Lakowicz, H. Szmacinski, K. Nowaczyk, K. W. Berndt, and M. Johnson, "Fluorescence lifetime imaging," *Anal. Biochem.* **202**(2), 316–330 (1992).
24. S. Kumar, C. Dunsby, P. A. De Beule, D. M. Owen, U. Anand, P. M. Lanigan, R. K. Benninger, D. M. Davis, M. A. Neil, P. Anand, C. Benham, A. Naylor, and P. M. French, "Multifocal multiphoton excitation and time correlated single photon counting detection for 3-D fluorescence lifetime imaging," *Opt. Express* **15**(20), 12548–12561 (2007).
25. A. V. Zvyagin, X. Zhao, A. Gierden, W. Sanchez, J. A. Ross, and M. S. Roberts, "Imaging of zinc oxide nanoparticle penetration in

human skin *in vitro* and *in vivo*," *J. Biomed. Opt.* **13**(6), 064031 (2008).
26. B. Geusens, M. Van Gele, S. Braat, S. C. De Smedt, M. C. A. Stuart, T. W. Prow, W. Sanchez, M. S. Roberts, N. N. Sanders, and J. Lambert, "Flexible nanosomes (SECosomes) enable efficient siRNA delivery in cultured primary skin cells and in the viable epidermis of *ex vivo* human skin," *Adv. Funct. Mater.* **20**(23), 4077–4090 (2010).
27. Q. Zhang, P. Li, and M. S. Roberts, "Maximum transepidermal flux for similar size phenolic compounds is enhanced by solvent uptake into the skin," *J. Controlled Release* **154**(1), 50–57 (2011).
28. L. L. Lin, J. E. Grice, M. K. Butler, A. V. Zvyagin, W. Becker, T. A. Robertson, H. P. Soyer, M. S. Roberts, and T. W. Prow, "Time-correlated single photon counting for simultaneous monitoring of zinc oxide nanoparticles and NAD(P)H in intact and barrier-disrupted volunteer skin," *Pharm. Res.* **28**, 2920–2930 (2011).
29. T. W. Prow, J. E. Grice, L. L. Lin, R. Faye, M. Butler, W. Becker, E. M. Wurm, C. Yoong, T. A. Robertson, H. P. Soyer, and M. S. Roberts, "Nanoparticles and microparticles for skin drug delivery," *Adv. Drug Deliv. Rev.* **63**(6), 470–491 (2011).
30. C. A. Thorling, Y. Dancik, C. W. Hupple, G. Medley, X. Liu, A. V. Zvyagin, T. A. Robertson, F. J. Burczynski, and M. S. Roberts, "Multiphoton microscopy and fluorescence lifetime imaging provide a novel method in studying drug distribution and metabolism in the rat liver *in vivo*," *J. Biomed. Opt.* **16**, 086013 (2011).
31. Q. Yu and A. A. Heikal, "Two-photon autofluorescence dynamics imaging reveals sensitivity of intracellular NADH concentration and conformation to cell physiology at the single-cell level," *J. Photochem. Photobiol., B* **95**(1), 46–57 (2009).
32. H. D. Vishwasrao, A. A. Heikal, K. A. Kasischke, and W. W. Webb, "Conformational dependence of intracellular NADH on metabolic state revealed by associated fluorescence anisotropy," *J. Biol. Chem.* **280**(26), 25119–25126 (2005).
33. R. J. Dinis-Oliveira, J. A. Duarte, F. Remiao, A. Sanchez-Navarro, M. L. Bastos, and F. Carvalho, "Single high dose dexamethasone treatment decreases the pathological score and increases the survival rate of paraquat-intoxicated rats," *Toxicology* **227**(1–2), 73–85 (2006).
34. R. Weigert, M. Sramkova, L. Parente, P. Amornphimoltham, and A. Masedunskas, "Intravital microscopy: a novel tool to study cell biology in living animals," *Histochem. Cell Biol.* **133**(5), 481–491 (2010).
35. P. P. Provenzano, K. W. Eliceiri, and P. J. Keely, "Multiphoton microscopy and fluorescence lifetime imaging microscopy (FLIM) to monitor metastasis and the tumor microenvironment," *Clin. Exp. Metastasis* **26**(4), 357–370 (2009).
36. B. G. Wang, K. Konig, and K. J. Halbhuber, "Two-photon microscopy of deep intravital tissues and its merits in clinical research," *J. Microsc.* **238**(1), 1–20 (2010).
37. T. P. Theruvath, Z. Zhong, P. Pediaditakis, V. K. Ramshesh, R. T. Currin, A. Tikunov, E. Holmuhamedov, and J. J. Lemasters, "Minocycline and N-methyl-4-isoleucine cyclosporin (NIM811) mitigate storage/reperfusion injury after rat liver transplantation through suppression of the mitochondrial permeability transition," *Hepatology* **47**(1), 236–246 (2008).
38. H. Rehman, V. K. Ramshesh, T. P. Theruvath, I. Kim, R. T. Currin, S. Giri, J. J. Lemasters, and Z. Zhong, "NIM811 (N-methyl-4-isoleucine cyclosporine), a mitochondrial permeability transition inhibitor, attenuates cholestatic liver injury but not fibrosis in mice," *J. Pharmacol. Exp. Ther.* **327**(3), 699–706 (2008).
39. M. Rubart, "Two-photon microscopy of cells and tissue," *Circ. Res.* **95**(12), 1154–1166 (2004).
40. D. Ban, A. Kudo, S. Sui, S. Tanaka, N. Nakamura, K. Ito, M. Suematsu, and S. Arii, "Decreased Mrp2-dependent bile flow in the post-warm ischemic rat liver," *J. Surg. Res.* **153**(2), 310–316 (2009).
41. S. Demir and M. Inal-Erden, "Pentoxifylline and N-acetylcysteine in hepatic ischemia/reperfusion injury," *Clin. Chim. Acta* **275**(2), 127–135 (1998).
42. L. M. Colletti, S. L. Kunkel, A. Walz, M. D. Burdick, R. G. Kunkel, C. A. Wilke, and R. M. Strieter, "The role of cytokine networks in the local liver injury following hepatic ischemia/reperfusion in the rat," *Hepatology* **23**(3), 506–514 (1996).
43. A. Takano, Y. Shibayama, and K. Nakata, "The morphogenesis of the vacuolation of liver cells," *Liver* **4**(2), 97–104 (1984).
44. P. Sileri, S. Schena, S. Morini, C. Rastellini, S. Pham, E. Benedetti, and L. Cicalese, "Pyruvate inhibits hepatic ischemia-reperfusion injury in rats," *Transplantation* **72**(1), 27–30 (2001).
45. M. Naito, G. Hasegawa, Y. Ebe, and T. Yamamoto, "Differentiation and function of Kupffer cells," *Med. Electron. Microsc.* **37**(1), 16–28 (2004).
46. A. A. Heikal, "Intracellular coenzymes as natural biomarkers for metabolic activities and mitochondrial anomalies," *Biomark. Med.* **4**(2), 241–263 (2010).
47. A. D. Ormerod, P. Copeland, I. Hay, A. Husain, and S. W. Ewen, "The inflammatory and cytotoxic effects of a nitric oxide releasing cream on normal skin," *J. Invest. Dermatol.* **113**(3), 392–397 (1999).
48. J. Hughes and G. Gobe, "Identification and quantification of apoptosis in the kidney using morphology, biochemical and molecular markers," *Nephrology (Carlton)* **12**(5), 452–458 (2007).
49. J. J. Maher, "Exploring alcohol's effects on liver function," *Alcohol Health Res. World.* **21**(1), 5–12 (1997).
50. C. Mouta Carreira, S. M. Nasser, E. di Tomaso, T. P. Padera, Y. Boucher, S. I. Tomarev, and R. K. Jain, "LYVE-1 is not restricted to the lymph vessels: expression in normal liver blood sinusoids and down-regulation in human liver cancer and cirrhosis," *Cancer Res.* **61**(22), 8079–8084 (2001).
51. S. L. Arnaiz, S. Llesuy, J. C. Cutrin, and A. Boveris, "Oxidative stress by acute acetaminophen administration in mouse-liver," *Free Radic Biol. Med.* **19**(3), 303–310 (1995).
52. E. Barbiro, Y. Zurovsky, and A. Mayevsky, "Real time monitoring of rat liver energy state during ischemia," *Microvasc. Res.* **56**(3), 253–260 (1998).
53. N. S. Chandel, G. R. Budinger, S. H. Choe, and P. T. Schumacker, "Cellular respiration during hypoxia. Role of cytochrome oxidase as the oxygen sensor in hepatocytes," *J. Biol. Chem.* **272**(30), 18808–18816 (1997).
54. T. H. Chia, A. Williamson, D. D. Spencer, and M. J. Levene, "Multiphoton fluorescence lifetime imaging of intrinsic fluorescence in human and rat brain tissue reveals spatially distinct NADH binding," *Opt. Express* **16**(6), 4237–4249 (2008).
55. R. Niesner, B. Peker, P. Schlusche, and K. H. Gericke, "Noniterative biexponential fluorescence lifetime imaging in the investigation of cellular metabolism by means of NAD(P)H autofluorescence," *ChemPhysChem* **5**(8), 1141–1149 (2004).
56. M. C. Skala, K. M. Riching, D. K. Bird, A. Gendron-Fitzpatrick, J. Eickhoff, K. W. Eliceiri, P. J. Keely, and N. Ramanujam, "*In vivo* multiphoton fluorescence lifetime imaging of protein-bound and free nicotinamide adenine dinucleotide in normal and precancerous epithelia," *J. Biomed. Opt.* **12**(2), 024014 (2007).
57. T. Schroeder, H. Yuan, B. L. Viglianti, C. Peltz, S. Asopa, Z. Vujaskovic, and M. W. Dewhirst, "Spatial heterogeneity and oxygen dependence of glucose consumption in R3230Ac and fibrosarcomas of the Fischer 344 rat," *Cancer Res.* **65**(12), 5163–5171 (2005).
58. A. S. Kannerup, H. Gronbaek, P. Funch-Jensen, R. L. Jorgensen, and F. V. Mortensen, "The influence of preconditioning on metabolic changes in the pig liver before, during, and after warm liver ischemia measured by microdialysis," *Hepatol. Int.* **3**(1), 310–315 (2009).
59. K. Theodoraki, N. Arkadopoulos, G. Fragulidis, D. Voros, K. Karapanos, M. Markatou, G. Kostopanagiotou, and V. Smyrniotis, "Transhepatic lactate gradient in relation to liver ischemia/reperfusion injury during major hepatectomies," *Liver Transpl.* **12**(12), 1825–1831 (2006).